RESIDUAL OIL SATURATION UNDER MIXED-WET CONDITIONS: A DIRECT COMPARISON BETWEEN INDIANA LIMESTONE AND ITS MICROFLUIDIC ANALOGUE

Yukie Tanino, Magali Christensen, Xanat Zacarias Hernandez
School of Engineering, University of Aberdeen, UK

This paper was prepared for presentation at the International Symposium of the Society of Core Analysts held in Vienna, Austria, 27 August – 1 September 2017.

ABSTRACT

We present laboratory measurements of residual oil saturation established by secondary waterflood in packed beds of crushed calcite assembled in a microfluidic channel under mixed-wet conditions. The measurements are compared with analogous measurements in Indiana limestone cores using the same test fluids and comparable injection rates. The wettability is characterized by the advancing contact angle of the flood water on a mineralogically representative substrate submerged in the oil phase, which ranged from θ_a = 90° to 160°.

While residual oil saturation is larger in the microfluidic analogue than the limestone cores over the full range of θ_a considered presently, its dependence on θ_a is qualitatively similar for both media and is well described by a concave-up quadratic function. Maximum recovery occurs at moderately oil-wet conditions of θ_a = 130° in Indiana limestone and 120° in its microfluidic analogue. These findings demonstrate that salient features of oil/brine flow through O(10)cm-long cores are conserved in two-dimensional microfluidic models under conditions considered presently.

INTRODUCTION

Salient features of waterflood oil recovery under mixed-wet conditions where the oil-contacted grain surfaces are strongly oil-wet are well established. However, there is no consensus on the optimal wettability for waterflood oil recovery. While some laboratory studies and pore network simulators report the dependence of oil recovery on contact angle, their findings are contradictory, with maximum recovery reported at neutral wettability in some studies [1, 2] and under strongly oil-wet conditions in others [3].

In this paper, we focus on residual oil saturation, S_{or}, established by secondary waterflood from high initial oil saturation under capillary-dominated conditions, and its dependence on contact angle under mixed-wet conditions. We compare measurements in Indiana

limestone and a quasi-monolayer of marble grains assembled in a microfluidic channel. Numerical simulation is used to quantify the impact of capillary end effects. An empirical model is proposed to describe the dependence of S_{or} on the advancing contact angle on a mineralogically representative substrate, θ_a, which is valid over the range $90° \leq \theta_a < 160°$.

METHODS

Porous Medium

The cross-sections of the limestone and its microfluidic analogue captured by X-ray micro tomography (Xradia Versa) are shown in Figure 1. The Indiana limestone cores had a mean porosity and permeability of $\phi = 0.15$ and $k = (6.5 \pm 2.7) \times 10^{-15}$ m^2, respectively, and were $L = 3.5$ in.-long and 1.5 in. in diameter [4]. Mercury injection porosimetry and NMR data are available in Refs. [4, 5].

The microfluidic analogue was a quasi-monolayer bed of crushed marble from Carrara, Italy, with a mean equivalent diameter of 53 ± 24 μm [6], packed in a $W = 1200$ μm-wide, $H = 55$ μm-deep channel etched in soda lime (Dolomite Centre Ltd.). The grains were prepared and wet-packed following the protocol described in Ref. [6] with minor modifications. The mean porosity of the marble packed bed was estimated from X-ray micro tomography scans of a microfluidic analogue to be $\phi = 0.27$. The length of the packed beds ranged from $L = 1280$ to 2440μm.

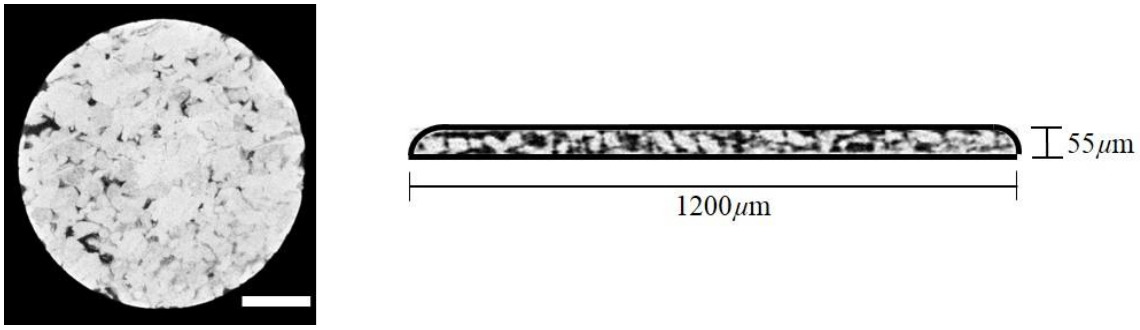

Figure 1. A two-dimensional cross-section of three-dimensional X-ray scans of Indiana limestone (left, [5]) and its microfluidic analogue (right). The diameter of the limestone sample is 5 mm; the white horizontal bar depicts 1200 μm, the width of the microfluidic analogue. Voxel size is 2.7551 μm for the limestone and 2.9586 μm for the microfluidic analogue.

Fluids

The aqueous phase was a solution of 5wt.% sodium chloride and 1wt.% potassium chloride saturated in limestone, as used previously [4, 5, 7, 8]. Four oils were considered: 6.6×10^{-2} M solutions of cyclohexanecarboxylic acid, cyclohexanepropionic acid, cyclohexanebutyric acid, and cyclohexanepentanoic acid in *n*-decane. In-situ adsorption of these acids render Indiana limestone and its microfluidic analogue mixed wet to different degrees [4, 10]. In the lab-on-a-chip measurements, the oils were dyed with Oil Red O

(ORO) to facilitate visualization; details are presented in Ref. [9]. At ambient conditions, the dynamic viscosity of the brine is μ_w = 1.087 mPa s. The dynamic viscosity of the dyed and undyed oils range from μ_o = 1.027 to 1.116 mPa s [10] and μ_o = 0.880 to 0.910 mPa s [4], respectively.

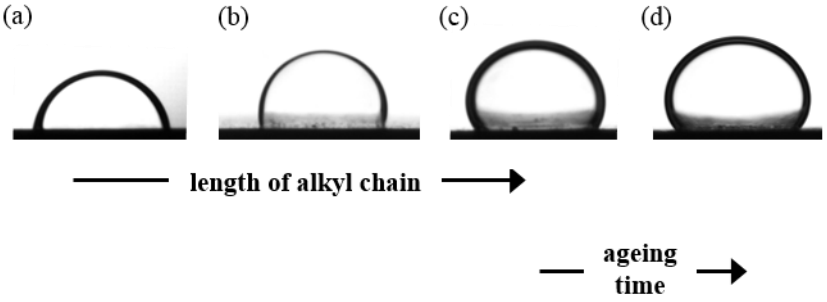

Figure 2. A drop of brine on a polished marble substrate that had been pre-equilibrated in brine then submerged in 6.6 × 10^{-2} M cyclohexanecarboxylic acid (a), cyclohexanebutyric acid (b), and cyclohexanepentanoic acid (c, d) for t_a = 1h (a-c) or 75h (d). The drop volumes are approximately the same in all images.

Contact Angle

Each oil/brine pair is characterised by the advancing contact angle, θ_a, on a mineralogically representative substrate that had been submerged in the test oil for ageing time t_a relevant to the displacement experiments (e.g., Fig. 2). Because cores were saturated in oil for much longer than the duration required for contact angles to asymptote (~ 50h [4]), their wettability is represented by equilibrium (long-time) values of θ_a. For dyed oils, t_a was matched to the duration that the microfluidic analogues were saturated in the test oil prior to waterflooding.

Table 1. Interfacial tension and advancing contact angle of each oil/brine pair. The reported uncertainty is standard error of the mean. All measurements were collected at ambient temperature.

	θ_a [°]		σ [mN/m]	
oil	**with dye (t_a) [10]**	**without dye [4]**	**with dye [10]**	**without dye [4]**
6.6 × 10^{-2} M cyclohexanecarboxylic acid	89 ± 3° (1h)	108 ± 0°	29.7	33.10 ± 0.003
6.6 × 10^{-2} M cyclohexanepropionic acid	N/A	127 ± 2°	22.5	28.50 ± 0.006
6.6 × 10^{-2} M cyclohexanebutyric acid	113 ± 2° (1h)	134 ± 2°	23.0 ± 0.1	23.67 ± 0.006
6.6 × 10^{-2} M cyclohexanepentanoic acid	140 ± 2° (1h)	150 ± 0.6°	19.3 ± 0.1	16.50 ± 0.010
	155 ± 5° (75h)			

The values of θ_a for the test oils and t_a corresponding to the experiments reported in this paper are summarized in Table 1. In the discussion that follows, all θ_a are rounded to the nearest 5°. Also reported are the interfacial tensions, σ, for each oil/brine pair.

Displacement Experiments

Two techniques were used to measure the remaining oil saturation as a function of time during waterfloods, $S_o(t)$: lab-on-a-chip methods [9] and conventional corefloods [4]. In both methods, each experiment comprised three stages: complete saturation of the porous medium with the brine, primary drainage, and waterflood at constant Darcy velocity, U_w. To remove ambiguity in the wettability of the system, cores and microfluidic analogues were not reused once they were exposed to oils containing organic acid.

Corefloods

Details of the coreflood apparatus and procedure can be found in Ref. [4]. The key steps were as follows:

1. Each core was alternately evacuated and flushed with gaseous CO_2 to remove air, then flushed with degassed brine to fully saturate it.
2. The test oil was injected into the core at constant pressure to establish initial oil saturation, S_{oi}, using the porous plate method.
3. Up to 100 pore volumes (pv) of degassed brine was injected at constant U_w = 30 μm/s in one experiment and 1.5 or 3.0 μm/s (= 0.43 and 0.85 ft/d) in all others.

The corresponding microscopic capillary number,

$$\mathrm{Ca} = \frac{\mu_w U_w}{\sigma}, \tag{1}$$

varied between Ca = 5×10^{-8} and 1×10^{-6}. The corresponding macroscopic capillary number [11],

$$\langle \mathrm{Ca} \rangle = \frac{\mu_w U_w L/k}{P_b}, \tag{2}$$

where $P_b = 2\sigma \cos\theta_a / r_{p,b}$ and (S_w, $r_{p,b}$) corresponds to the inflection point in the mercury injection (drainage) capillary pressure curves, varied between 0.43 and 6.3 (Table 2). Data to date suggest that S_{or} is not a strong function of U_w within this range [4, 8, 12].

S_{oi} and S_{or} were determined by mass balance on the core. In this paper, we consider maximum S_{oi} (≈ 0.9) only.

Lab-on-a-Chip Experiments

The lab-on-a-chip method combines, with modifications, the coreflood protocol of Tanino & Blunt [7] and the lab-on-a-chip protocol developed by Bowden et al. [6]:

1. The packed bed was first saturated with the brine to establish connate water saturation.
2. Oil was injected until a uniform oil saturation of $S_{oi} \cong 1$ was established. Fresh oil was circulated through the packed bed for t_a = 1h or 75h to allow the acid in the oil phase to render grain surfaces oil-wet to different degrees.

3. Brine was injected at U_w = 26μm/s (= 7.3ft/d) using a high precision syringe pump; the corresponding capillary number ranges from Ca = 9×10^{-7} to 1×10^{-6} and $\langle \mathrm{Ca} \rangle$ = 2×10^{-3} to 7×10^{-2} (Table 2).

Because we do not have a method for measuring $P_c(S_w)$ in the microfluidic rock analogues at this time, the breakthrough capillary pressure was estimated as

$$P_b = J(S_{w,b})\sigma \cos\theta_a \sqrt{\frac{\phi}{k}}, \tag{3}$$

where $J(S_{w,b})$ is the Leverett-J scaling

$$J(S_{w,b}) = \frac{P_c(S_{w,b})}{\sigma \cos\theta_a}\sqrt{\frac{k}{\phi}} \tag{4}$$

corresponding to the inflection point in primary imbibition oil/water capillary pressure curve in a packed column of mixed-wet spheres [13].

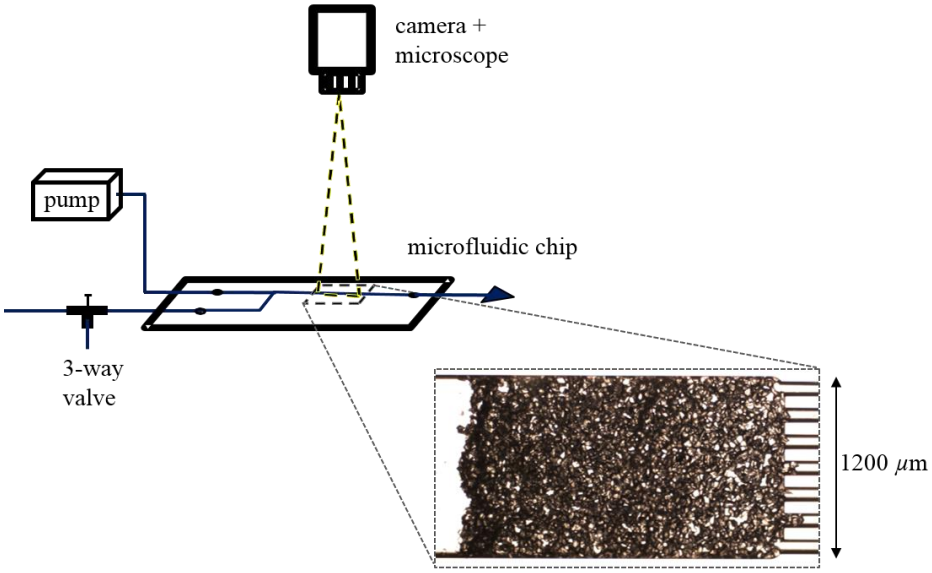

Figure 3. Setup for the lab-on-a-chip experiments. The chip is back lit from below. Adapted from Tanino et al. [8].

Flow Visualization

The evolution of the depth-integrated oil distribution inside the packed bed was captured using a high-speed camera coupled to an optical microscope at a resolution of 2.4 to 4.0 μm/pix; the chip was lit from below (Fig. 3).

The distribution of oil within the packed bed and its evolution were determined as follows:

1. The red channel field of the acquired still images, $i_R(x, y, t)$, was subtracted from the green channel field, $i_G(x, y, t)$.
2. A 3 × 3 median filter was applied to the resulting $i_G - i_R$ field.

3. A segmentation threshold, $i_c(y)$, was determined for each half-width of the packed bed.

The remaining oil saturation at a given instance as a fraction of the initial oil saturation was determined as:

$$\frac{S_o(t)}{S_{oi}} = \frac{n_o(t)}{n_o(t<0)}, \tag{5}$$

where n_o is the number of pixels in the packed bed for which i_G-$i_R < i_c(y)$; $t = 0$ corresponds to the time when water first enters the packed bed. All post-processing was performed using MATLAB (Mathworks, Ltd.). Additional details are provided in Ref. [9].

Capillary end effects are a concern in microfluidic experiments and, indeed, oil saturation tends to be larger near the downstream end of the packed bed than the upstream end. However, this phenomenon is observed at $\theta_a < 90°$ also, which suggests that it is largely due to imperfections in the channel cross-section at the downstream end of the packed bed rather than the capillary discontinuity. For simplicity, the last 300 μm (= 5.5H) of the packed bed was excluded from consideration to prevent end effects from unrealistically increasing the estimated $S_o(t)$ (e.g., Fig. 4, white rectangle). As will be shown below, the reduction in $S_o(t)$ that arises from expanding the excluded region to 550 μm (= 10H) falls within experimental uncertainty (Fig. 6, dashed-dotted).

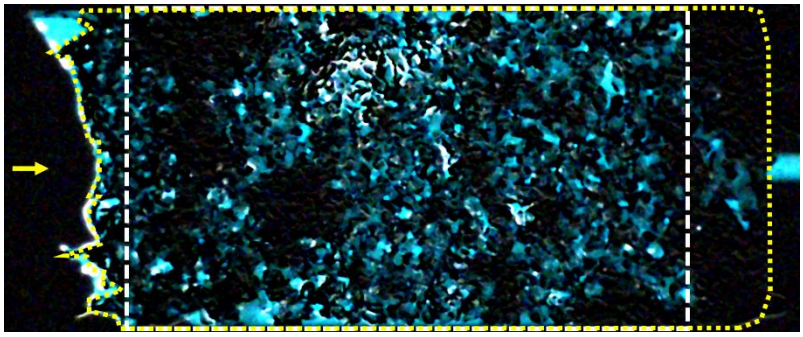

Figure 4. A microfluidic analogue at residual oil saturation for $\theta_a = 155°$; $S_{or}/S_{oi} = 0.50$. An image at initial oil saturation has been subtracted from the image and a 3 × 3 median filter applied; the bright pixels represent invading water. The yellow polygon demarcates the boundaries of the packed bed. The white dashed box demarcates the region over which $S_o(t)$ is evaluated. Mean flow is left to right.

Numerical simulation

Numerical simulations of the corefloods were performed using CYDAR™ (CYDAREX). First, waterflood (secondary imbibition) capillary pressure, $P_c^B(S_w)$, and relative permeability, $k_r^B(S_w)$, curves of a Berea sandstone pore network from Ref. [5] were predicted for each oil/brine combination using a two-phase pore network simulator developed by Valvatne & Blunt [14]; details of the pore network are available in Ref. [5]. To account for differences in S_{or}, water saturation was rescaled as

$$S_w^* = \frac{S_w - (1 - S_{oi})}{(1 - S_{or}) - (1 - S_{oi})}. \quad (6)$$

Similarly, P_c^B was scaled using the Leverett-J function, i.e.,

$$P_c(S_w^*) = P_c^B(S_w^*)\sqrt{\frac{k^B/\phi^B}{k/\phi}}, \quad (7)$$

where superscript B denotes properties of the Berea sandstone pore network. $P_c(S_w^*)$ and $k_r^B(S_w^*)$ were used as input parameters for the simulations.

RESULTS

Figure 5 presents the residual oil saturation distribution along the length of the Indiana limestone core as predicted by the simulator for each θ_a. At all θ_a considered, the oil saturation at the upstream end of the core (x = 0) agrees with the "true" S_{or}, i.e., the oil saturation corresponding to k_{ro} = 0, to within -0.09% to 0.07%. As x increases, oil saturation remains uniform within the first x < 5 mm (θ_a = 110°) to 5 cm (150°), then increases gradually with increasing x until $x/L \approx 0.95$. Finally, in the last 4 mm of the core, oil saturation increases sharply to $\approx S_{oi}$ to accommodate the P_c = 0 boundary condition at x = L. Because capillary end effects are constrained to a small region, the core-averaged residual oil saturation is only 2 to 4% larger than the residual oil saturation at the upstream end of the core, $S_{or}(x = 0)$.

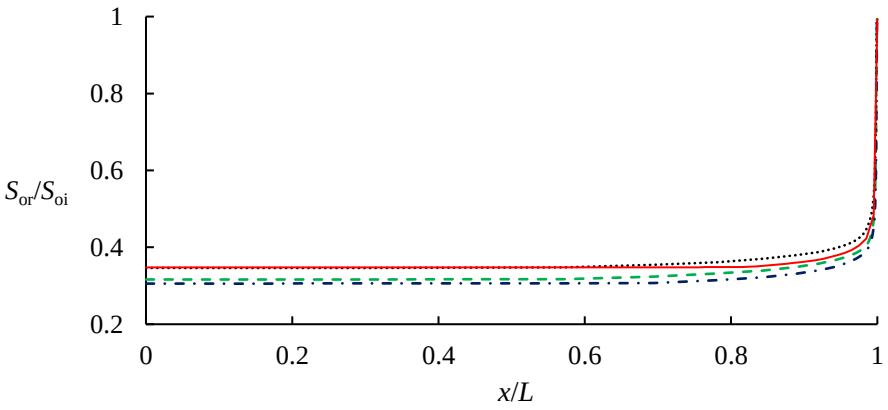

Figure 5. Residual oil saturation in Indiana limestone cores at θ_a = 110° (black dotted), 125° (green dashed), 135° (blue dashed-dotted), and 150° (red solid line). Mean flow is left to right. L = 8.9cm; ϕ = 0.15; k = 6.597mD; S_{oi} = 0.9.

Figure 6 presents the evolution of the remaining oil saturation from Indiana limestone (blue) and its microfluidic analogue (red, magenta) under weakly oil-wetting and strongly oil-wetting conditions. Time $\tilde{t}$ is defined from the onset of waterflood in units of cumulative pv of brine injected. During any waterflood, S_o decreases as waterflood progresses until it asymptotes to its residual state. The constant, long-time value is taken

to be S_{or} for Indiana limestone. For simplicity, S_{or} in the microfluidic analogues is taken to be S_o time-averaged over $\tilde{t} = 30 \pm 0.5$ after water breakthrough.

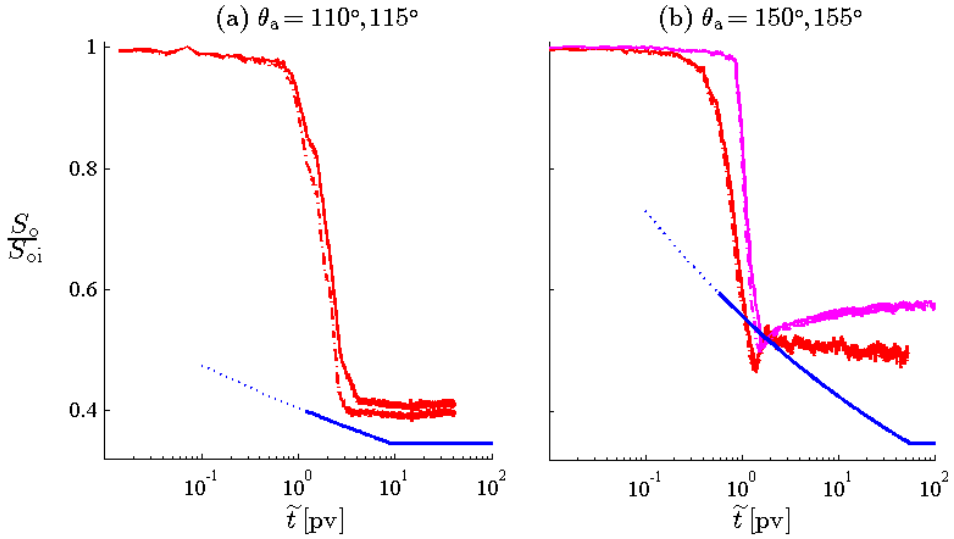

Figure 6. Evolution of the remaining oil saturation during waterflood at θ_a = 110°/115° (a) and 150°/155° (b) in cores (blue) and microfluidic analogues (red, magenta). Recovery from cores are represented by the best-fit power functions to data [4]. For microfluidic analogues, solid and dashed-dotted lines depict saturation excluding the last 300 and 550μm of the packed beds, respectively.

Table 2. Summary of experimental conditions.

	θ_a	⟨Ca⟩		ϕ	S_{or} / S_{oi}
porous medium		**min.**	**max.**		
Indiana limestone [4, 7]	108 ± 0°	0.63	0.69	0.149 – 0.155	0.35 ± 0.008
	127 ± 2°	0.54	6.3	0.143 – 0.154	0.32 ± 0.02
	134 ± 2°	0.43	1.3	0.139 – 0.156	0.31 ± 0.02
	150 ± 0.6°	1.4	1.5	0.133 – 0.139	0.35 ± 0.01
microfluidic analogue	89 ± 3°	7×10^{-2}		-	0.52
	113 ± 2°	3×10^{-3}		-	0.41 ± 0.03
	140 ± 2°	2×10^{-3}		-	0.45 ± 0.02
	155 ± 5°	2×10^{-3}		-	0.58 ± 0.03
		3×10^{-3}		-	0.50

Figure 7 presents S_{or} as a fraction of the OOIP as a function of θ_a. In both Indiana limestone and the microfluidic analogue, residual saturation displays a non-monotonic dependence on contact angle. In the former, S_{or}/S_{oi} decreases with increasing contact angle from S_{or}/S_{oi} = 0.35 at θ_a = 110° to S_{or}/S_{oi} = 0.31 ± 0.02 at 135°, then increases back to S_{or}/S_{oi} = 0.35 ±

0.01 at θ_a = 150° (squares). Similarly, S_{or}/S_{oi} decreases from S_{or}/S_{oi} = 0.52 at θ_a = 90° to S_{or}/S_{oi} = 0.41 ± 0.03 at θ_a = 115°, then increases to S_{or}/S_{oi} = 0.54 ± 0.04 at θ_a = 155° in the microfluidic analogue (circles). The data are well described by the best-fit quadratic function in the least-squares sense (dotted lines):

$$\frac{S_{or}}{S_{oi}} = 8.3\times10^{-5}\theta_a^{\,2} - 0.021\theta_a + 1.7 \tag{8}$$

and

$$\frac{S_{or}}{S_{oi}} = 1.1\times10^{-4}\theta_a^{\,2} - 0.026\theta_a + 2.0 \tag{9}$$

for Indiana limestone and its microfluidic analogue, respectively. For the same θ_a, S_{or}/S_{oi} in the microfluidic analogues exceeds that in Indiana limestone cores by 17% to 47% over the full range of θ_a considered presently, with the fractional difference increasing monotonically with θ_a.

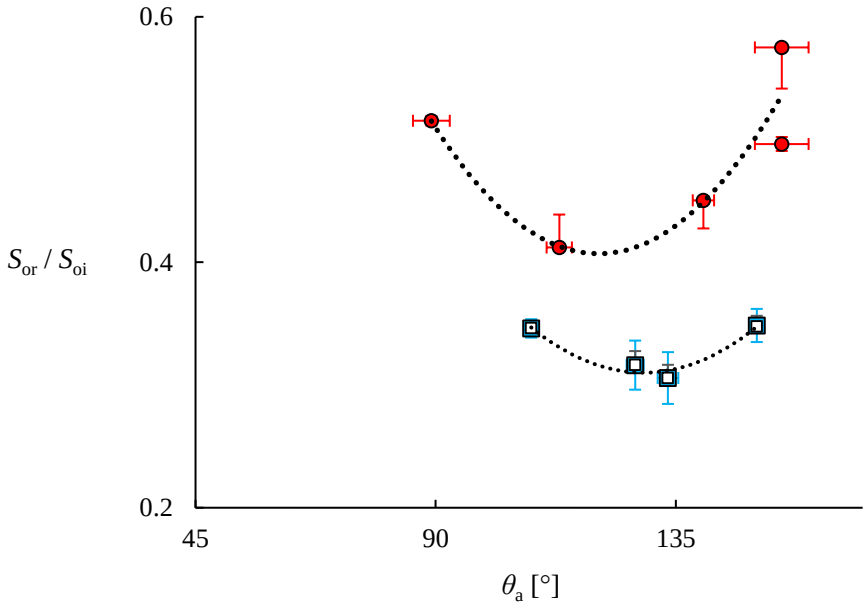

Figure 7. Residual oil saturation in Indiana limestone cores (blue squares; [4]) and microfluidic analogues (red circles). Each marker represents a single experiment for the microfluidic analogues and the average over two or three independent corefloods for Indiana limestone. Horizontal bars depict standard errors of the mean. Vertical bars depict the standard errors of the mean for Indiana limestone and the uncertainty in the segmentation threshold for microfluidic analogues. Dotted lines depict polynomial functions of degree two fitted to data in the least squares sense [Eqs. (8, 9)]. Superposed are residual oil saturation at the upstream end of the core determined from numerical simulation (open squares); vertical bars depict the core-averaged S_{or} in the simulations.

As discussed above, capillary end effects tend to elevate the porous medium-averaged S_{or} at $\theta_a > 90°$. To demonstrate that the observed non-monotonic trend is not an experimental artefact arising from two competing mechanisms – a reduction in true S_{or} and an increase in capillary end effects – we consider the θ_a dependence of the simulated S_{or}. $S_{or}(x = 0)$

displays a concave-up dependence on θ_a similar to the core-averaged S_{or}, with the same optimal contact angle of $\theta_a = 130°$ (Fig. 7, open squares). The positive correlation between $S_{or}(x = 0)$ and θ_a at high θ_a in the simulations suggests that previous observations of such correlations in corefloods are not an experimental artefact. Furthermore, the occurrence of the same correlation in the present microfluidic experiments suggests that the non-monotonic dependence is a salient feature of multiphase flow in mixed-wet media at low $\langle \mathrm{Ca} \rangle$.

CONCLUSIONS

Residual oil saturation in two-dimensional packed beds of calcite grains and three-dimensional limestone cores under mixed-wet conditions were compared. The main findings are:

- S_{or} decreases, then increases as θ_a increases from 90° to 160° in both systems.
- The non-monotonic dependence is well described by a concave-up quadratic function.
- Optimal wettability (minimum S_{or}) occurs at moderately oil-wetting conditions.
- S_{or} was larger in the microfluidic analogue than in Indiana limestone cores over the full range of θ_a considered presently.
- Numerical simulations of the corefloods demonstrate that the positive correlation between S_{or} and θ_a at large θ_a is not a result of two competing mechanisms – a reduction in S_{or} and an increase in oil retention due to capillary end effects – but a true behaviour of S_{or}.

Ongoing laboratory work is focused on an analogous comparison of relative permeability of Indiana limestone [15] and its microfluidic analogue.

ACKNOWLEDGEMENTS

This paper contains work supported by the Royal Society Research Grant RG140009. XZH was supported by the National Council for Science and Technology, Mexico. MC was supported by the University of Aberdeen College of Physical Sciences scholarship. The authors gratefully acknowledge Hu Dong at iRock Technologies and Mehmet Kartal for the X-ray micro-computed tomography scans of Indiana limestone and its microfluidic analogue, respectively, Aleksei Gunkin (University of Aberdeen MSc Petroleum Engineering, 2015) for his insights which have guided the development of the segmentation algorithm used presently, and Guillaume Lenormand at CYDAREX for helpful suggestions on their software CYDAR™.

REFERENCES

1. Kennedy, H. T., E. O. Burja & R. S. Boykin (1955) An investigation of the effects of wettability on oil recovery by water flooding. *J. Phys. Chem*. 59(9), 867-869. doi: 10.1021/j150531a015.
2. Morrow, N. R., P. J. Cram & F. G. McCaffery (1973) Displacement studies in dolomite with wettability control by octanoic acid. *Soc. Petrol. Eng. J*. 13(4), 221-232. doi: 10.2118/3993-PA.
3. Owens, W. W. & D. L. Archer (1971) The effect of rock wettability on oil-water relative permeability relationships. *Soc. Petrol. Eng. J*. 23(7), 873-878. doi: 10.2118/3034-PA.
4. Christensen, M. & Y. Tanino (2017) Waterflood oil recovery from mixed-wet limestone: dependence on contact angle. *Energy Fuels*, 31(2), 1529-1535. doi: 10.1021/acs.energyfuels.6b03249.
5. Tanino, Y. & M. J. Blunt (2012) Capillary trapping in sandstones and carbonates: dependence on pore structure. *Water Resour. Res*. 48(8), W08525. doi: 10.1029/2011WR011712.
6. Bowden, S. A., Y. Tanino, B. Akamairo & M. Christensen (2016) Recreating mineralogical petrographic heterogeneity within microfluidic chips: assembly, examples, and applications. *Lab Chip* 24(16), 4677-4681. doi: 10.1039/C6LC01209D.
7. Tanino, Y. & M. J. Blunt (2013) Laboratory investigation of capillary trapping under mixed-wet conditions. *Water Resour. Res.* 49(7), 4311-4319. doi: 10.1002/wrcr.20344.
8. Tanino, Y., B. Akamairo, M. Christensen & S. A. Bowden (2015) Impact of displacement rate on waterflood oil recovery under mixed-wet conditions. In *Proc.*, International Symposium of the Society of Core Analysts. St. John's Newfoundland and Labrador, Canada, 16-21 August.
9. Tanino, Y., M. Christensen & X. Zacarias Hernandez (2017) Dynamic, pore-scale imaging of water invasion in microfluidic packed beds, *Appl. Sci*., in prep.
10. Christensen, M., X. Zacarias Hernandez & Y. Tanino (2017) Impact of Oil Red O on physical and interfacial properties of *n*-decane+acid solutions, in prep.
11. Hilfer, R. & P.-E. Oren (1996) Dimensional analysis of pore scale and field scale immiscible displacement, *Transp. Porous Med.* 22(1), 53-72.
12. Christensen, M. & Y. Tanino (2017) Capillary desaturation curves under mixed-wet conditions: a microfluidic study, in prep.
13. Murison, J. L. (2013) Wetting heterogeneities in porous media: Insights from experiments on the displacement of immiscible fluids, PhD thesis, Georg-August-Universität, Göttingen, Germany.
14. Valvatne, P. H. & M. J. Blunt (2004) Predictive pore-scale modeling of two-phase flow in mixed wet media. *Water Resour. Res.* 40(7), W07406. doi: 10.1029/2003WR002627.
15. Christensen, M. & Y. Tanino (2017) Enhanced permeability due to apparent oil/brine slippage in limestone and its dependence on wettability, *Geophys. Res. Lett*. doi: 10.1002/2017GL073603.